In vitro and in vivo degradation behavior of Mg–2Sr–Ca and Mg–2Sr–Zn alloys

Kai Chen[a,b,1], Xinhui Xie[c,d,1], Hongyan Tang[a,b], Hui Sun[a,b], Ling Qin[d], Yufeng Zheng[e], Xuenan Gu[a,b,*], Yubo Fan[a,b,f,**]

[a] Key Laboratory for Biomechanics and Mechanobiology of Ministry of Education, School of Biological Science and Medical Engineering, Beihang University, Beijing, 100083, China
[b] Beijing Advanced Innovation Centre for Biomedical Engineering, Beihang University, Beijing, 100083, China
[c] The Department of Orthopedics, ZhongDa Hospital, School of Medicine, Southeast University, Nanjing, 210009, China
[d] Department of Orthopaedics and Traumatology, The Chinese University of Hong Kong, Hong Kong National Research Center for Rehabilitation Technical Aids, Beijing, 100176, China
[e] Department of Materials Science and Engineering, College of Engineering, Peking University, Beijing, 100871, China
[f] National Research Center for Rehabilitation Technical Aids, Beijing, 100176, China

ABSTRACT

Magnesium alloys with integration of degradability and good mechanical performance are desired for orthopedic implants. In this paper, Mg–2Sr–Ca and Mg–2Sr–Zn alloys were prepared and the degradation as well as the bone response were investigated. Compared with the binary Mg–2Sr alloys, the addition of Ca and Zn improved the in vitro and in vivo corrosion resistance. Mg–2Sr–Ca and Mg–2Sr–Zn alloys exhibited more uniform corrosion and maintained the configuration of the implants 4 weeks post-implantation. The in vivo corrosion rates were 0.85 mm/yr for Mg–2Sr–Zn and 1.10 mm/yr for Mg–2Sr–Ca in comparison with 1.37 mm/yr for Mg–2Sr. The in vitro cell tests indicated that Mg–2Sr–Ca and Mg–2Sr–Zn alloys exhibited higher MG63 cell viability than Mg–2Sr alloy. Furthermore, these two alloys can promote the mineralization and new bone formation without inducing any significant adverse effects and this sound osteogenic properties suggest its attractive clinical potential.

1. Introduction

In recent years, magnesium (Mg) and its alloys have attracted the attention of many researchers and have been considered as potential materials used in bone repair applications due to their superior properties, including close elastic modulus to human bone, essential nutrient element, high mechanical performance and degradation in physiological environment [1–4]. It has been suggested that the degradation profile is one of the most crucial parameters for biodegradable Mg alloys, which might limit their clinical applications [2,5]. Besides, the corrosion mode (localized corrosion or uniform corrosion) has been reported to have a significant influence on the mechanical integrity of Mg alloys [6–8], especially for being used as load-bearing orthopedic implants.

Mg–Sr alloys have recently been considered as potential biodegradable materials used in orthopedic surgery mainly due to the effect of Sr on stimulating bone formation and decreasing bone resorption [9–12]. Gu et al. [9] have studied the in vitro and in vivo performance of the as-rolled Mg–Sr alloys with Sr addition ranging from 1 to 4 wt% and proved that the as-rolled Mg–2Sr alloy presented finer microstructure (23 μm in average grain size), highest ultimate tensile strength (213 MPa), slower degradation rate (0.37 mm/year) and superior osteogenic properties during 4 weeks implantation among other alloys. Bornapour et al. [10] also proved that the as-cast Mg-0.5Sr alloy displayed a slower degradation rate and no thrombosis occurrence during in vivo implantation (3 weeks) in comparison with other cast Mg–Sr alloys. Zhao et al. [11] conducted extrusion treatment on Mg–Sr series alloys and found that the extruded Mg-0.5Sr alloy presented better mechanical properties, suitable corrosion resistance and non-toxicity to MG63 cells. Recently, it has been reported that heat-treated Mg–1Sr alloys possess good mechanical performance and corrosion resistance [12]. It can be expected that Mg–Sr alloy system exhibit good

biocompatibility and possess great potential to be used as biodegradable bone implants.

In order to further enhance the corrosion resistance, mechanical properties and biocompatibility of Mg–Sr alloys, Ca and Zn elements have been added as alloying element. Ca is one of the most abundant elements in human body, and it is the main component of hydroxyapatite [13–15]. Besides, the calcium phosphate formed during *in vivo* degradation process can provide a suitable environment for bone mineralization [16]. Zn is also an essential trace element and it involves many physiological metabolic processes in human body [17,18]. It plays a significant role in regulation of gene express, anti-atherosclerosis function, synthesis of nucleic acid and protein, promotion effect on nervous system, etc. [19,20]. Moreover, the addition of little amount of Ca and Zn is reported to have a prominent effect on refining microstructure of Mg alloys [21,22], which is beneficial to improving the mechanical properties and corrosion resistance simultaneously. Therefore, some Mg–Sr–Ca and Mg–Sr–Zn alloys have been prepared and investigated [23–25]. Bornapour et al. [23] successfully prepared Mg-0.3Sr-0.3Ca alloy and the results indicated that it has a higher corrosion resistance than binary Mg-0.6Ca and Mg-0.5Sr alloys. Harpreet et al. [24] studied the mechanical and *in vitro* degradation behavior of three ternary Mg-xZn-0.5Sr (x = 2, 4, 6 wt%) alloys and found that the addition of Zn can lead to the increase of yield and ultimate strength. Moreover, the addition of Zn in Mg–Sr–Ca alloy is found to both promote the growth of osteoblasts and improve antibacterial properties [25]. The previous study systematically investigated the *in vitro* degradation of Mg–Sr based alloys. While it is known that Mg based alloys usually exhibit quite different *in vivo* degradation performance from *in vitro*, mainly due to the complicated physiological environment. Therefore, it is necessary to further investigate the *in vivo* degradation behavior and bone response of Mg–Sr–Ca and Mg–Sr–Zn alloys to promote their clinical use.

In this study, we have successfully prepared the as-rolled Mg–2Sr–Ca and Mg–2Sr–Zn alloys based on our previous reports [9]. The *in vitro* and *in vivo* degradation behavior, cell viability, alkaline phosphatase activity (ALP) and histological evaluation were studied and compared to those of Mg–2Sr alloys. The results in this paper will promote the comprehension and applications of Mg–2Sr–Ca and Mg–2Sr–Zn alloys.

2. Materials and methods

2.1. Materials

The cast Mg–2Sr, Mg–2Sr–Ca and Mg–2Sr–Zn ingots in this study were prepared by traditional cast method. The pure Mg (99.98%), Mg–10%Sr master alloy, Mg–10%Ca master alloy and pure Zn (99.99%) were melted in a high purity graphite crucible under the protection of a mixed gas atmosphere of SF_6 (1 vol%) and CO_2 (balance). After being heated at 750 °C for 30 min, the melt was poured into a steel mold preheated to 300 °C. The actual chemical compositions of three cast alloys were analyzed by inductively coupled plasma atomic emission spectrometry (ICP-AES) (Leeman Labs, Hudson, NH), as shown in Table 1. The as-cast ingots were cut into 6 mm thick plates and then pre-heated at 400 °C for 3 h, followed by rolling down to 1.5 mm thick sheets. The reduction in thickness of the plates was 0.2 mm in a single pass and the plates were reheated to 400 °C for 10 min between each

pass. Disk samples with a size of $10 \times 10 \times 1.5$ mm^3 were cut along the rolling direction of the rolled sheet plates. The disk samples were ground by silicon carbide sandpaper up to 2000#, followed by ultrasonic cleaning in acetone, absolute ethanol and distilled water (10 min for each step). Then, these samples were sterilized by ultraviolet and then used for cytotoxicity tests. In addition, the cylindrical rods ($\Phi 0.7 \times 5$ mm^3) were also cut from the rolling direction of the rolled plates as intramedullary nails for animal experiments.

2.2. Electrochemical measurement

The potentiodynamic polarization (PDP) behavior of three alloys were measured by a standard three electrode electrochemical workstation (Autolab, Metrohm, Switzerland) at the temperature of 37 ± 0.5 °C in Hank's solution. The detailed chemical composition of Hank's solution can be found in Ref. [9]. The prepared samples, saturated calomel electrode (SCE) and a platinum plate were adopted as working, reference and auxiliary electrode, respectively. The polarization studies were conducted at a scan rate of 1 mV/s from -2.0 to -1.0 V (vs. SCE). The corrosion current of three alloys were obtained by the Tafel extrapolation according to ASTM-G102-89 standard [26] and the corrosion rate (CR) of alloys can be calculated by Eq [1]:

$$CR = 3.27 \times 10^{-3} \frac{I_{corr} EW}{\rho} \tag{1}$$

where CR is the corrosion rate of alloys (mm/yr), I_{corr} represents the corrosion current density (μA/cm^2), EW is the equivalent weight of these alloys and ρ is the density of metals (g/cm^3). The determination of PDP curves of each alloys was measured by three parallel samples.

2.3. Immersion test

The immersion tests were also carried out in Hank's solution with temperature being 37 °C according to ASTM-G31-72 standard [27]. The ratio of sample area to Hank's solution is 1 cm^2: 20 ml. After 20 days immersion, the samples were removed from Hank's solution, gently rinsed with distilled water and dried in air. The corrosion surface morphology and chemical composition of corrosion products were measured by scanning electron microscope (SEM, Hitachi S-4800, Japan) equipped with an energy dispersive spectrometer (EDS). Moreover, the components of corrosion products were also analyzed by an X-ray diffractometer (Rigaku DMAX 2400, Japan) using CuK$_\alpha$ radiation. To evaluate the corrosion rates of three alloys, the released hydrogen volume was recorded every day and the total hydrogen volume duration was 20 days. Therefore, the corrosion rates of alloys can be calculated as following [28,29]:

$$CR = \frac{8.76 \times 10^4 \Delta W}{A \times t \times \rho} \tag{2}$$

$$\Delta W = 1.085 V_H \tag{3}$$

where ΔW is the weight loss after 20 days immersion (g), A represents the sample surface area (cm^2), t is immersion time (h), ρ is the density of alloys (g/cm^3) and V_H is the total volume of hydrogen evolution (L).

Table 1
The chemical compositions of as-rolled Mg–2Sr, Mg–2Sr–Ca and Mg–2Sr–Zn alloys. (wt.%).

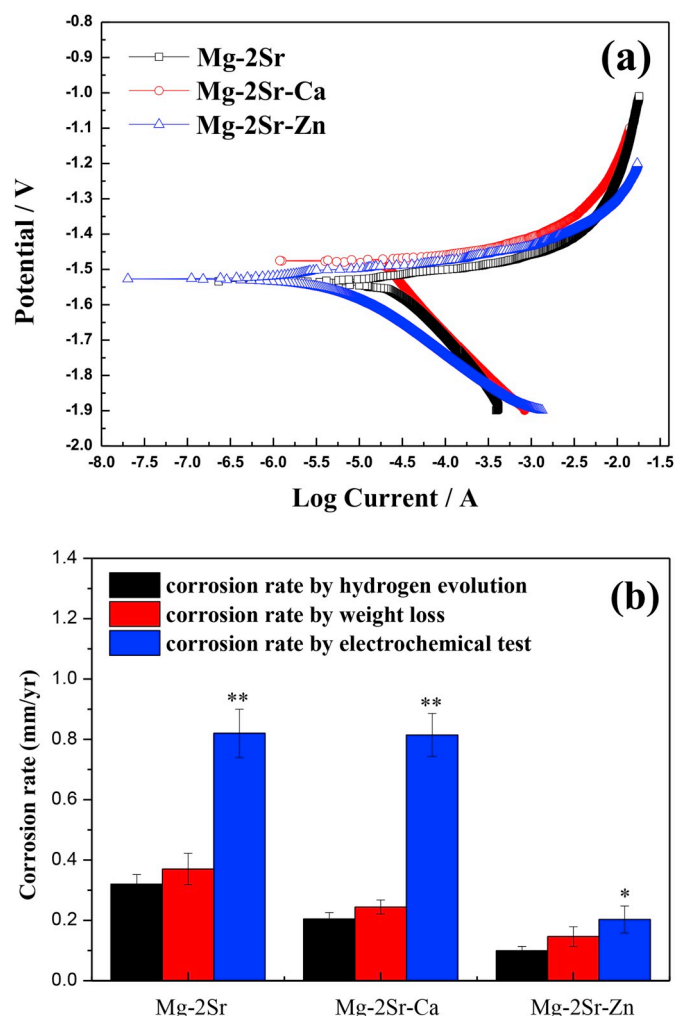| Alloys	Sr	Ca	Zn	Fe	Si	Ni	Cu	Mg
Mg–2Sr	1.80	–	–	< 0.005	< 0.001	< 0.001	< 0.001	Bal.
Mg–2Sr–Ca	1.96	0.85	–					
Mg–2Sr–Zn	1.87	–	0.84					

Fig. 1. (a) The polarization curves of Mg–2Sr, Mg–2Sr–Ca and Mg–2Sr–Zn alloys and (b) the corrosion rate calculated by hydrogen evolution, weight loss and electrochemical approaches with Mg–2Sr alloy as control group. *$P < 0.05$ and **$P < 0.01$.

2.4. Cytotoxicity and ALP tests

Human osteosarcoma MG63 cells were adopted to evaluate the cytocompatibility of three alloys and the detail cell culture method can be found in our previous report [9]. The cytocompatibility of three alloys was measured by indirect contact method and the extracts were collected by soaking samples into cell culture medium (serum free) with the surface area to medium ratio of 1 ml/cm^2 in a humidified atmosphere with 5% CO_2 at 37 °C for 72 h. The cell cytotoxicity tests were carried out by MTT assay according to previous report [9]. The extract media has been refreshed before adding MTT, thus the interference from the ions (Mg, Sr, Zn, Ca) on the absorbance value could be avoided. Afterwards, the absorbance of each well was inspected by a microplate reader (Bio-Rad 680) at 570 nm.

For the ALP tests, MG63 cells were incubated in 24-well plates with a density of about 3000 cells in each well. After 24 h incubation, the medium was replaced with extracts and then cultured for 7 days. Afterwards, the differentiation behavior of MG63 cells was inspected by measuring ALP activity. The cultured cells were gently rinsed with phosphate buffer solution for three times and lysed in 0.1% Triton X-100 by freezing and thawing for two cycles. Then the ALP activity was measured using p-nitrophenyl phosphate (pNpp) as the substrate (Sigma, St Louis, MO). The entire reaction last for 1 h and was stopped

by adding 1 M NaOH solution. The quantity of produced pNpp was measured at 410 nm by a microplate reader and the total protein content was inspected by a BCA Protein Assay Kit (Sigma).

2.5. Animal experiment

2.5.1. Implantation surgery

Animal experimental protocol was approved by the Animal Ethics Committee of the Chinese University of Hong Kong (Ref No. 10/049/MIS). Twelve 3-month old C57bl/6 mice were randomly assigned to three groups (n = 4). Four mice were used as control group. Before implantation surgery, these mice were anesthetized by ketamine (75 mg/kg) and xylazine (10 mg/kg) and the left knee was cleaned by tincture of iodine (25 g/L) and ethanol (70%). Afterwards, the machined cylindrical rods (Φ0.7 × 5 mm^3, sterilized by ethylene oxide) were implanted into the bone medullary cavity along the axis of the shaft from the distal femora. After implantation surgery, these mice were housed in an animal care laboratory. In addition, the predrilled bone tunnel without implants was settled as blank control. To make a comparison, the *in vivo* implantation process and the data of Mg–2Sr alloys can be found in Ref. [9]. The change of serum Mg, Sr, Ca and Zn were measured 4 weeks post-surgery by ICP-AES.

2.5.2. Radiographic and micro-CT observation

After implantation, the distal femora of post-surgery mice were inspected by sequential radiographs (30 kV, 3 s) every week. Moreover, an *in vivo* micro computerized tomography (micro-CT, viva CT40, Scanco Medical AG, Brüttisellen, Switzerland) was adopted to monitor the variation trend of the distal femora at 0, 1, 2, 3 and 4 weeks after operation. The scanning accuracy of the micro-CT is 20 μm for each step. The change of the implants in the bone tunnel was measured using our published protocol [30]. Two-dimensional (2-D) images were acquired directly from the scans and the three-dimensional (3-D) structure was reconstructed using the volume of interest (VOI), with an optimized threshold used to isolate the bone and materials from the background. The volume changes of the implants, the thickness and density of the peri-implant cortical bone were measured based on the obtained 2-D and 3-D micro-CT results [9]. The *in vivo* corrosion rates of Mg–2Sr–Ca and Mg–2Sr–Zn alloys can be acquired as following:

$$CR_{vivo} = (V_t - V_0)/At \tag{4}$$

Where CR_{vivo} is the degradation rate of alloys, V_0 represents the volume of alloy measured by micro-CT at 0 week, V_t is the volume of the alloy at different time points, A is the initial implant surface area and t is the implantation time.

2.5.3. Histological evaluations

4 weeks after operation, the mice were euthanized and the femora were harvested, followed by soaking in 10% buffered formalin. Then the gradient alcohol dehydration was carried out and the femora were embedded and polymerized in methylmethacrylate resin. The mounted femora were cut by a diamond saw (Leica SM2500E) into 120 μm undecalcified sections, followed by grounding and polishing to a thickness of 70 μm. The polished section was then stained with Stevenel's blue and Van Gieson's picro fuchsin, and the morphology was observed by a Nikon ECLIPSE LV100ND optical and fluorescence microscope. To label the newly formed bone, the fluorescent staining agents calcein green (5 mg/kg) and xylenolorange (90 mg/kg) were injected subcutaneously at 14 and 4 days, respectively, before the mice were killed following our published protocol [9].

2.6. Statistical analysis

Statistical analysis was conducted by SPSS 21.0 software and the difference was calculated based on the analysis of variance (ANOVA) and Tukey test. All tests were repeated at least for three times.

Table 2
The obtained polarization data of as-rolled Mg–2Sr, Mg–2Sr–Ca and Mg–2Sr–Zn alloys.

Alloy	E_{corr} (V vs SCE)	I_{corr} (μA/cm^2)	β_c (V dec)
Mg–2Sr	−1.53 ± 0.02	21.41 ± 3.52	0.19 ± 0.04
Mg–2Sr–Ca	−1.47 ± 0.02	18.42 ± 3.83	0.16 ± 0.03
Mg–2Sr–Zn	−1.53 ± 0.01	4.68 ± 1.03	0.08 ± 0.02

3. Results

3.1. In vitro degradation

To evaluate the corrosion behaviors of as-rolled Mg–2Sr, Mg–2Sr–Ca and Mg–2Sr–Zn alloys, the electrochemical approaches and immersion tests were carried out and the corrosion rates of three alloys were determined by hydrogen evolution, weight loss and potentiodynamic polarization tests, respectively.

Fig. 1a shows the polarization curves of as-rolled Mg–2Sr, Mg–2Sr–Ca and Mg–2Sr–Zn alloys and it can be discovered that the corrosion potential (E_{corr}) of Mg–2Sr–Ca alloy presents more positive than that of Mg–2Sr and Mg–2Sr–Zn alloys (as shown in Table 2). Based on the cathode Tafel extrapolation method, the polarization data of three alloys can be obtained, as displayed in Table 2. Despite the difference in E_{corr}, the corrosion current densities (I_{corr}) of Mg–2Sr–Ca (18.42 μA/cm^2) and Mg–2Sr–Zn (4.68 μA/cm^2) are apparently lower than that of Mg–2Sr alloy (21.41 μA/cm^2). In addition, as depicted in Fig. 1b, the corrosion rates measured by three methods present the same variation trend and it indicates that the corrosion resistance of three alloys is in the order of Mg–2Sr < Mg–2Sr–Ca < Mg–2Sr–Zn, corresponding to the electrochemical results as mentioned above. The corrosion rates of as-rolled Mg–2Sr–Zn and Mg–2Sr–Ca alloys determined by mass loss are 0.147 mm/yr and 0.244 mm/yr, respectively and which is about 39.6% and 65.9% of the as-rolled Mg–2Sr alloy. The enhanced corrosion resistance of Mg–2Sr–Ca and Mg–2Sr–Zn alloys can be mainly ascribed to the finer microstructure after alloying with Ca

and Zn element based on previous report [9,31,32].

Fig. 2 shows the corrosion surface morphologies of Mg–2Sr, Mg–2Sr–Ca and Mg–2Sr–Zn alloys after immersion in Hank's solution for 20 days. It can be observed that the three alloys all show a uniform corroded surface with some irregular precipitates distributed on the sample surface (Fig. 2a–c). Moreover, there are also some micro cracks exists on the corroded surface layer due to the dehydration during drying. The representative EDS analysis (Fig. 2c and d) indicates that the corroded surface layer of Mg–2Sr–Ca and Mg–2Sr–Zn alloys mainly consists of Mg, O, P, and Ca elements. It suggests that the surface corrosion products are mainly composed of hydroxide, phosphates and carbonates. The similar EDS results can also be found in Mg–2Sr (not shown) according to previous studies [9,25]. The XRD analysis demonstrates the precipitation of Mg(OH)$_2$, while no diffraction peaks arising from the second phase Mg$_{17}$Sr$_2$ [9] are detected due to the corrosion product layer. In addition, it is hard to distinguish the phosphate and carbonate based precipitates from the XRD pattern because of its relative low content.

3.2. Cytotoxicity

Fig. 3a shows the viability of MG63 cell after cultured in Mg–2Sr, Mg–2Sr–Ca and Mg–2Sr–Zn alloys extraction medium for 1, 3 and 5 days. The cell viability cultured by Mg–2Sr–Ca or Mg–2Sr–Zn alloy extracts at day 1 was significantly higher than that of Mg–2Sr, which can be mainly attributed to the slower corrosion rate of Mg–2Sr–Ca and Mg–2Sr–Zn alloys. With the culture period extended, Mg–2Sr–Ca and Mg–2Sr–Zn groups exhibit comparable cell viability to that of Mg–2Sr group. Compared with the ALP activity of Mg–2Sr alloy (Fig. 3b), it seems there exists no significant difference in Mg–2Sr–Ca and Mg–2Sr–Zn alloys extracts.

3.3. In vivo degradation and biocompatibility

3.3.1. X-ray and micro-CT analysis

Fig. 4 shows the X-ray radiographs of mice femora with and without implantation of Mg–2Sr–Ca and Mg–2Sr–Zn alloy pins. All mice
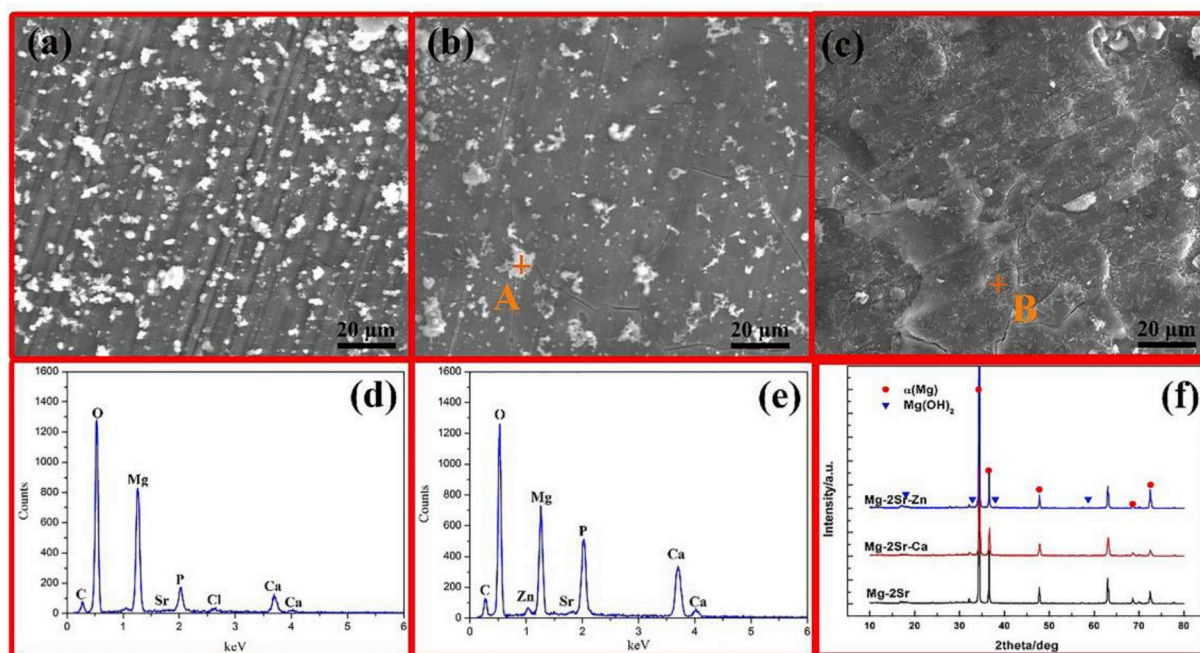

Fig. 2. The corrosion surface morphologies of (a) Mg–2Sr alloy, (b) Mg–2Sr–Ca alloy, (c) Mg–2Sr–Zn alloy after immersion in Hank's solution for 20 days, (d) the EDS result of the marked point (point A) in Fig. 2b and (e) the point B in Fig. 2c, (f) the XRD patterns of these alloys after 20 days immersion tests.
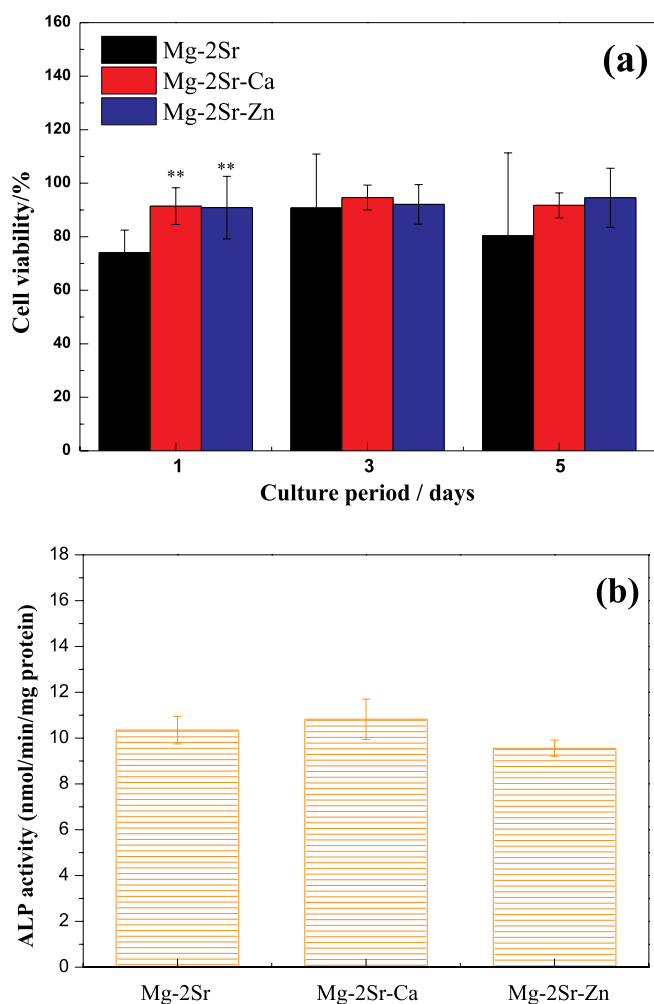
Fig. 3. (a) MG63 cell viability of Mg–2Sr, Mg–2Sr–Ca and Mg–2Sr–Zn alloys for 1, 3 and 5 days, (b) ALP activity of Mg–2Sr, Mg–2Sr–Ca and Mg–2Sr–Zn alloys extracts. **$P < 0.01$.

rods, corresponding to the immersion and electrochemical results shown above. As the rods degrades, the bone remodeling can be found at the surface of distal femora during the implantation period (Fig. 5). By week 4 we can observe the integration of newly formed bone and a relative smooth surface of the distal femur (Fig. 5).

Furthermore, the implants volume, cortical bone thickness and bone mineral density (BMD) were quantified and plotted in Fig. 7. It can be observed that the volume loss of Mg–2Sr–Ca and Mg–2Sr–Zn implants is 51.71% and 39.81%, respectively, which is smaller than that of the Mg–2Sr implants (64.48% volume loss after 4 weeks) and indicating a better *in vivo* corrosion resistance. Three alloys all have a promoted effect on the new bone formation after 4 weeks implantation. The significant increment of cortical bone thickness ($p < 0.01$) can be found since 2 weeks post-surgery. Mg–Sr–Ca alloy shows nearly twice the cortical bone thickness at week 4 as the blank control. An increase of BMD value can also be discovered in Mg–2Sr–Zn and Mg–2Sr–Ca compared to the non-implanted control group.

3.3.2. Histological evaluations

Fig. 8 shows the histological cross-sectional graphs of the mice distal femora after 4 weeks implantation. Both Mg–2Sr–Ca and Mg–2Sr–Zn rods (denoted by yellow circle) maintained their central integrity and some of which were surrounded by fibrous tissue (denoted by red arrows). There were also some degradation products or the debris from the corroded implants (denoted by blue arrows) dispersed in the trabecular area, the bone marrow cavity as well as in the fibrous tissue. In addition, a thicker cortical bone in Fig. 8d and f suggests a promotion effect of new bone formation in both Mg–2Sr–Ca and Mg–2Sr–Zn alloy group.

Fig. 9 displays the corresponding fluorescence images of the cross-sections of the mice distal femora with new bone formation in the diaphyseal and trabecular region. In comparison with control group, thicker cortical bone occurs in both Mg–2Sr–Ca and Mg–2Sr–Zn alloy group (Fig. 9g and k), especially beneath the periosteum. There were more newly formed bone trabeculae in the Mg–2Sr–Ca and Mg–2Sr–Zn alloy groups as compared to the non-implanted control group. In Mg–2Sr–Ca alloy group, the endosteal new bone formation can be observed, which is not found in other two groups and indicating a better bone formation ability of Mg–2Sr–Ca alloy.

Fig. 10 shows the elemental distributions in cross sections of the femoral shaft with the as-rolled Mg–2Sr–Zn alloy 4 weeks post-implantation. From the elemental mapping, the residual implants with high concentration of Mg can be clearly observed without major cracking inside the rods. Around the implants, it indicates a gradient descent of Mg concentration. The elemental distribution of Ca and P confirm the extensive mineralization within the medullary cavity. The elemental distribution of Sr and Zn is not shown due to their low concentrations which exceed the resolution limit of the EDS mapping technique. Thus the elemental line scan has been carried out to figure out the elemental distribution change from the residual implants to the cortical bone (Fig. 10b). A thin mineralized layer rich in Ca and P is shown at the implant-tissue interface within the medullary cavity, which is accordance with the green ring surrounding the residual implants in Fig. 9. In addition, we also observe slightly higher concentration of Sr and Zn in this area. Similar to the elemental distribution maps for Mg–2Sr–Zn alloy, the distribution of CaP based minerals in the bone tunnel and the thicker cortical bone are also observed for Mg–2Sr–Ca alloy.

4 weeks post-implantation, the serum ion concentrations of mice implanted with Mg–2Sr–Ca rods are 23.24 ± 0.203 μg/ml for Mg, 0.224 ± 0.007 μg/ml for Sr and 72.10 ± 0.336 μg/ml for Ca. The serum ion concentrations of mice implanted with Mg–2Sr–Zn rods are 25.20 ± 0.035 μg/ml for Mg, 0.203 ± 0.007 μg/ml for Sr and 0.445 ± 0.007 μg/ml for Zn. The serum ion concentration for the

survived with normal mobility after implantation of Mg–2Sr–Ca and Mg–2Sr–Zn alloy pins and there is no inflammation around the implantation sites. Mg–2Sr–Ca and Mg–2Sr–Zn alloy pins can maintain their original shape under radiographs and micro-CT observations (Fig. 5) mainly due to their relatively low *in vivo* degradation rate. Besides, the black shadows can be inspected around the implantation sites. This phenomenon can be mainly attributed to degradation-induced hydrogen, which can't be absorbed or diffuse in a short period and results in gas shadows in radiographs [33]. The gas shadow is more obvious from the micro-CT analysis (Fig. 6). After 1 week, periosteal reaction and reactive hyperplasia of bone occurred around the cortical bone of distal femora (orange arrows), indicating that both alloys have a promotion effect on new bone growth.

The 3-D reconstruction of the femora with implants (Figs. 5) and 2-D cross-sectional micro-CT photographs (Fig. 6) clearly show the degradation of the Mg–2Sr–Ca and Mg–2Sr–Zn alloy rods. Localized degradation of the implants at the rod surface can be found in both the cortical and trabecular bone areas 1 week post-operation. The degradation proceeds with the central region of rods maintaining its integrity 4 weeks post-operation. The *in vivo* degradation of Mg–2Sr–Ca and Mg–2Sr–Zn alloy rods differs in different places of the femora (Fig. 5), exhibiting more rapid degradation in the bone marrow cavity region than the distal regions. In addition, *in vivo* degradation of Mg–2Sr–Zn alloy rods is much slower than that of Mg–2Sr–Ca alloy
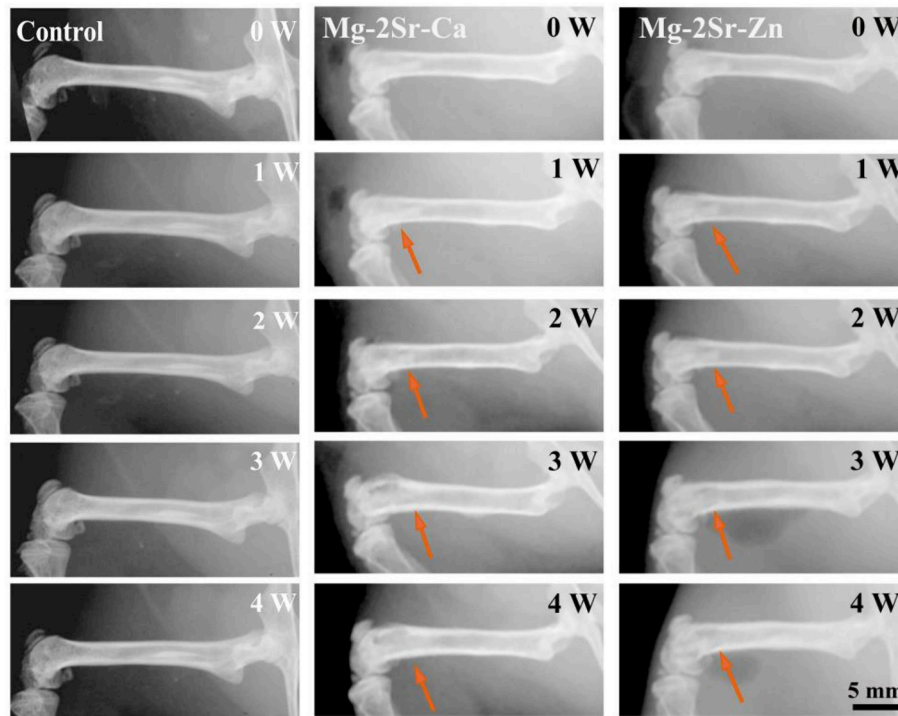
Fig. 4. X-ray photographs of mice femora with and without implantation of Mg–2Sr–Ca and Mg–2Sr–Zn rods.

control group are 25.16 ± 0.224 µg/ml for Mg, 0.217 ± 0.007 µg/ml for Sr, 74.72 ± 0.152 µg/ml for Ca and 0.469 ± 0.007 µg/ml for Zn. It can be seen that the degradation of the Mg–2Sr–Ca and Mg–2Sr–Zn alloys did not raise the Mg^{2+}, Sr^{2+}, Ca^{2+} and Zn^{2+} ions concentrations in the blood 4 weeks post-implantation.

4. Discussion

Biodegradable Mg alloys have been considered as potential materials to be used as orthopedic implants. Nevertheless, the fast corrosion rate and unpredictable corrosion mode will lead to the premature loss
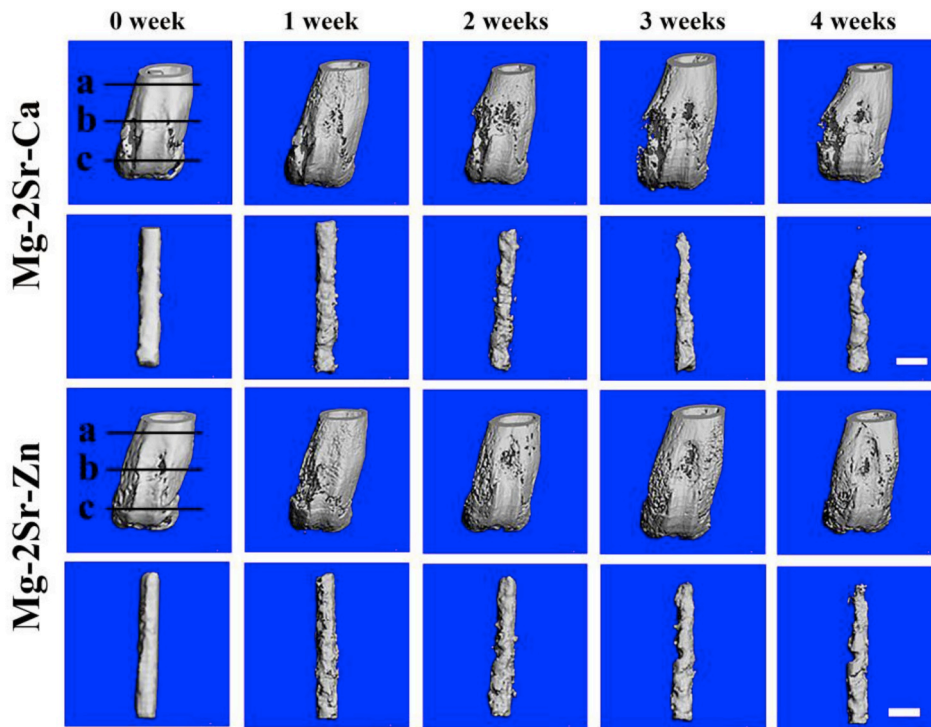

Fig. 5. 3-D reconstruction photographs of mice femora and intramedullary Mg–2Sr–Zn and Mg–2Sr–Ca pins at different time poins after surgery. The bar length is 1.0 mm.
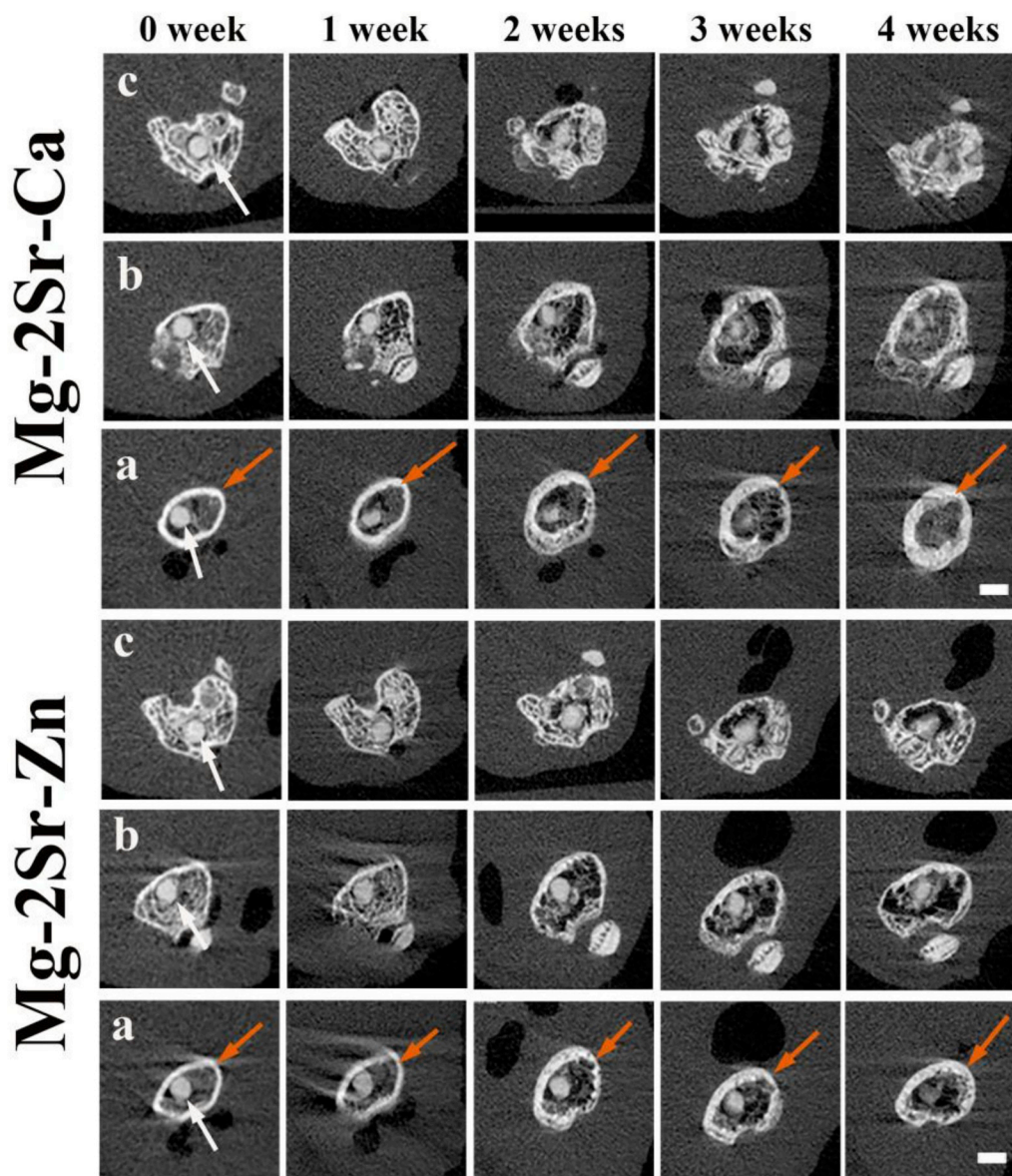
Fig. 6. 2-D cross-sectional pictures of post-surgery mice femora in different places, corresponding to the straight lines in Fig. 5 (0 week) with embedded Mg–2Sr–Ca and Mg–2Sr–Zn pins (white arrows) at different post-surgery time points. (a) Proximal part of the distal femur; (b) middle part of the distal femur; (c) distal part of the distal femur. The bar length is 1.0 mm.

of mechanical integrity of implants, which limit the clinical applications of biodegradable Mg alloys [34]. Therefore, many efforts have been made to enhance the corrosion resistance of biodegradable Mg alloys. In this study, ternary Mg–2Sr–Ca and Mg–2Sr–Zn alloys have been investigated to explore the effect of Ca and Zn addition on the *in vitro* and *in vivo* degradation, cytotoxicity and bone response of Mg–2Sr alloy.

Both electrochemical behavior and immersion results indicate that the Mg–2Sr–Zn alloy exhibits slower corrosion rate than the Mg–2Sr–Ca alloy, followed by the Mg–2Sr alloy, as shown in Fig. 1b. The corrosion rates are 0.147 mm/yr for Mg–2Sr–Zn and 0.244 mm/yr for Mg–2Sr–Ca alloys, which show 34.1–60.4% reduction in comparison with Mg–2Sr alloys (0.37 mm/yr). Erinc et al. [35] suggested that the *in vitro* corrosion rate of ideal biodegradable Mg alloys should be less than 0.5 mm/yr, indicating that both Mg–2Sr–Zn and Mg–2Sr–Ca alloys are potential materials to be used as biodegradable implants. In comparison with Mg–2Sr alloy, the improved corrosion resistance of Mg–2Sr–Zn and Mg–2Sr–Ca alloys can be mainly ascribed to the refined

microstructure after adding the alloying element of Ca and Zn, according to the microstructure of our previous reports [9,31,32]. The effect of micro alloyed Ca or Zn on refining microstructure and the enhancement of corrosion resistance have also been reported in Mg-Si-Ca [36] and Mg–Zn alloys [37]. It can be inspected from Fig. 1b that the corrosion rate measured by electrochemical tests is much higher than those evaluated by the hydrogen evolution or weight loss tests. It is because that the weight-loss or hydrogen evolution rate is actually an average result of a corroding samples over a certain period of time, while the instantaneous corrosion rate is obtained by the electrochemical techniques. This phenomenon is also observed in the corrosion tests of Mg–Sr alloy [9] and AZ91 alloy [38].

Figs. 11–12 compares the 3-D micro-CT reconstruction of the femora of mice with Mg–2Sr, Mg–2Sr–Ca and Mg–2Sr–Zn alloy rods 4 weeks post-operation as well as their *in vivo* degradation rates. The *in vivo* degradation rates of Mg–2Sr–Zn (0.85 mm/yr) and Mg–2Sr–Ca (1.10 mm/yr) are slower than that of Mg–2Sr alloys (1.37 mm/yr), corresponding to the *in vitro* corrosion results in Fig. 1b. Moreover, the
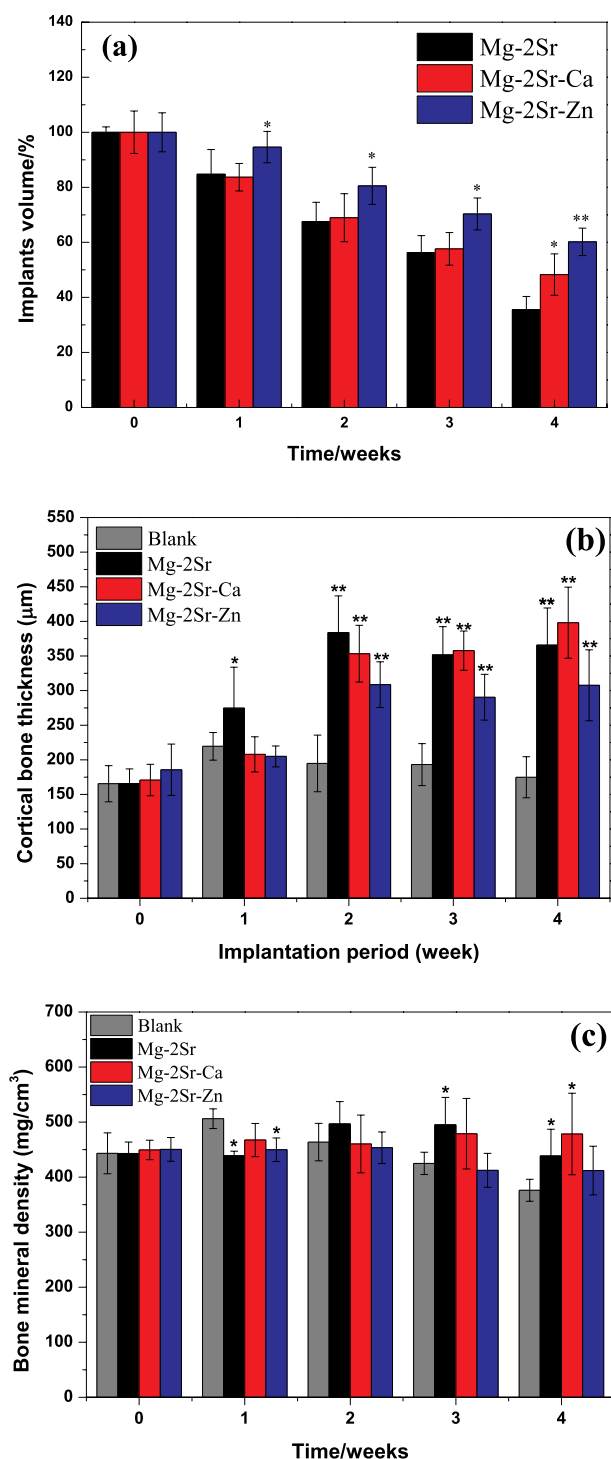
Fig. 7. (a) Implants volume, (b) cortical bone thickness and (c) bone mineral density in the Mg–2Sr, Mg–2Sr–Ca and Mg–2Sr–Zn alloys group at different implantation intervals. *$P < 0.05$ and **$P < 0.01$."

ternary alloys exhibit a more uniform *in vivo* degradation mode, which could benefit in keeping mechanical integrity of implants and avoid premature fracture before bone healing. Interestingly, the i*n vivo* degradation rates are significantly higher than their respective degradation rates *in vitro*, which is not expected. Since the *in vivo* degradation rate is generally considered to be slower than that measured via *in vitro* immersion or electrochemical test [39]. Sanchez et al. [39] reported a

comprehensive review to compare the *in vitro* and *in vivo* degradation of Mg alloys and found the *in vivo* degradation rate could be as much as nine times lower when compared with the *in vitro* ones. An explanation for the accelerated *in vivo* degradation in the present study may involve the anatomical regions where the implant is placed [40]. The intramedullary area is rich in vasculature and body fluids, which can refresh microenvironment surrounding the implants more rapidly and results in the accelerated degradation. It is in agreement with previous studies that reported faster *in vivo* degradation, when compared with their *in vitro* counterparts, for Mg–2Sr [9], Mg-5.25Zn-0.6Ca [41] and Mg–6Zn [42] intramedullary implants and a tubular Mg-0.5Sr stent [10].

The degradation of Mg–2Sr–Ca and Mg–2Sr–Zn implants showed a massive cortico-periosteal reaction and resulted significantly thicker cortical bone (Figss. 8–9), revealing their osteogenesis effect. The Mg ion-induced bone formation has been widely reported in the previous studies [40,41], while excessive Mg releasing also increases osteoclastogenesis and results in less bone formation, as seen for pure Mg and ZX50 [32,43]. In the present study, Mg–2Sr–Ca implants show much thicker cortical bone (Fig. 7b) even with a more rapid *in vivo* degradation, most likely due to the more leaching of Sr and Ca ions. As Sr can enhance new bone formation by activating Wt/Catenin signaling and decrease bone resorption, the continued Sr ion release with the degradation of implants could achieve the stimulatory effect on new bone growth [9,32,44]. Occasionally fibrous encapsulation develops around the both implants (Fig. 8c and f). This observation seems to be in line with other Mg based alloys and is a normal feature to develop predominantly around solid implants [40,43]. In addition, we also found the fibrous region contains high concentrations of Ca and P, evidenced by the EDS and the hyper dense fluorescence around implants (Figss. 9–10). This calcium phosphate minerals could possibly create a more bone-mimicking interface for osteoblasts attaching and spreading. Jiang et al. [45] found an improved bone marrow derived mesenchymal stem cells adhesion on Mg–Ca–Sr alloy as compared with Mg–Sr alloy. However, the detachment between the trabecular bone and the residual implant surface is present (Figs. 8c and 9e) as a result of the very fast degradation of Mg–2Sr–Ca alloy. For Mg–2Sr–Zn, it shows a relative appropriate *in vivo* degradation as well as the bone response, evidenced by the apposition of new trabeculae along the residual Mg–2Sr–Zn surface (Fig. 8e). In addition, the Zn-based implants have shown a beneficial effects on new bone formation [46], which may verify the promoting effect of Mg–2Sr–Zn alloy on new bone formation as collateral evidence.

The *in vivo* degradation rate is 1.1 mm/yr for Mg–2Sr–Ca and 0.85 mm/yr for Mg–2Sr–Zn alloys. Thus the daily release of Mg^{2+}, Sr^{2+} and Ca^{2+} ions of a Mg–Sr–Ca rod ($\Phi 0.7 \times 5$ mm^3) can be calculated by the surface area and degradation rate and they are approximately 60.6 mg, 1.2 mg and 0.5 mg, respectively. The daily release of Mg^{2+}, Sr^{2+} and Zn^{2+} ions from one Mg–2Sr–Zn rod is about 48.2 mg, 0.9 mg and 0.4 mg. It has been suggested that the recommended daily allowance (RDA) of Mg, Sr, Ca and Zn are 240–420 mg/day [47], 800–1200 mg/day [48], 4–5 mg/day [10] and 8–11 mg/day [18], respectively. The figured value of Mg, Sr, Ca, and Zn is negligible compared with the upper limit of RDA, ensuring a good biosafety and indicating good potential as biodegradable materials. It is in line with the not significantly changed Mg^{2+}, Sr^{2+}, Ca^{2+} and Zn^{2+} ions concentrations in the blood for Mg–2Sr–Ca and Mg–2Sr–Zn after 4 weeks implantation.

In summary, we have successfully prepared as-rolled Mg–2Sr–Ca and Mg–2Sr–Zn alloys to use as orthopedic implants. The *in vitro* and *in vivo* corrosion resistance of Mg–2Sr–Ca and Mg–2Sr–Zn alloys are both improved in comparison with previous Mg–2Sr alloys. Both alloys present good cell viability and sound osteogenic properties, showing great potential as clinical orthopedic implant materials.
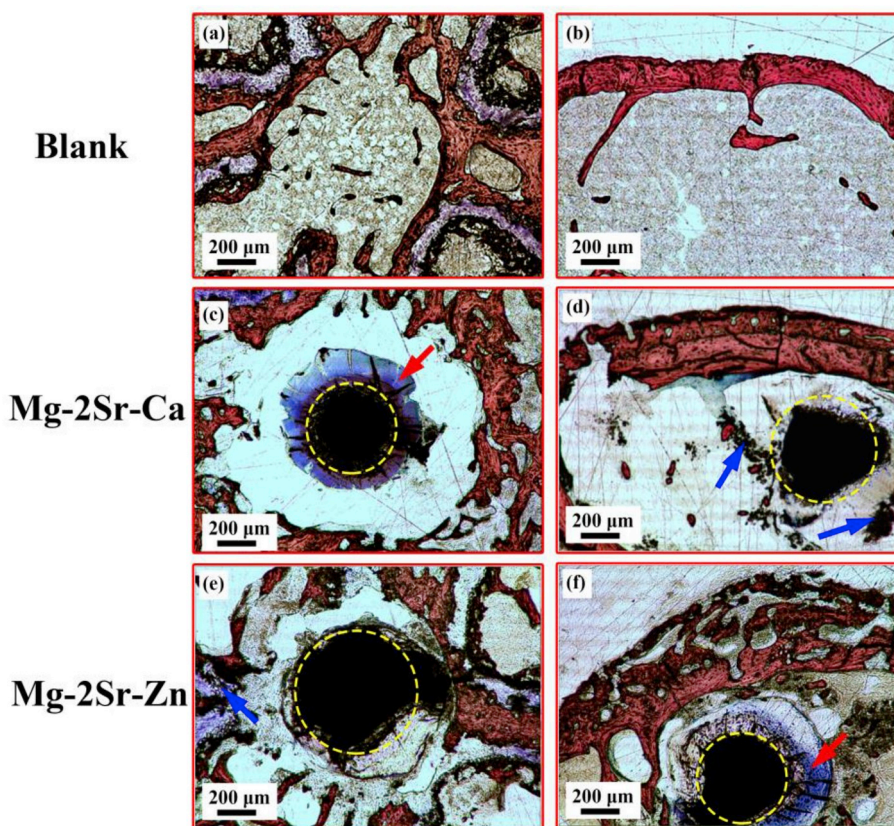
Fig. 8. Histological cross-sections graphs of the mice distal femora 4 weeks post-implantation, (a–b) non-implanted control group, (c–d) Mg–2Sr–Ca and (e–f) Mg–2Sr–Zn alloy group. The yellow circles, red arrows and blue arrows represent the implants, fibrous tissue and degradation products, respectively.

5. Conclusions

In this study, we developed as-rolled Mg–2Sr–Ca and Mg–2Sr–Zn alloys for orthopedic applications. The *in vitro* and *in vivo* degradation behavior and biocompatibility of Mg–2Sr–Ca and Mg–2Sr–Zn alloys were investigated. The following conclusions can be drawn:

1. The *in vitro* degradation rates of Mg–2Sr–Ca and Mg–2Sr–Zn alloys

are 0.244 mm/yr and 0.147 mm/yr, which is about 65.9% and 39.6% of the as-rolled Mg–2Sr alloys. The Mg–2Sr–Ca and Mg–2Sr–Zn alloys present uniform corrosion with hydroxide, phosphates and carbonates deposited on the surface.

2. The *in vitro* cell tests indicated that Mg–2Sr–Ca and Mg–2Sr–Zn alloys showed promoted MG63 cell viability in comparison with Mg–2Sr alloy.

3. The *in vivo* corrosion resistance of Mg–2Sr–Ca and Mg–2Sr–Zn alloys
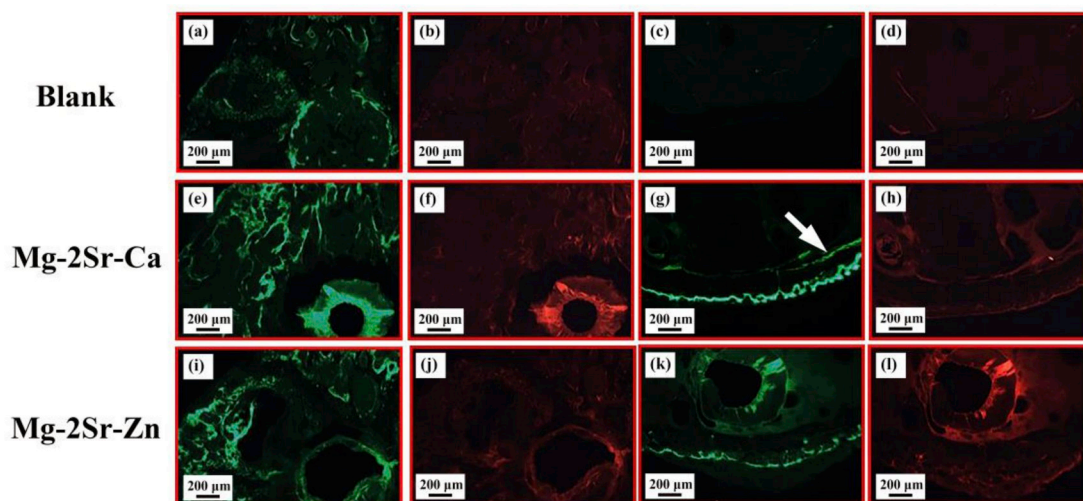

Fig. 9. Fluorescence images of the cross-sections of the mice distal femora 4 weeks post-implantation, (a–d) non-implanted control group, (e–h) Mg–2Sr–Ca and (i–l) Mg–2Sr–Zn alloy group. The white arrow indicates the endosteal new bone formation.
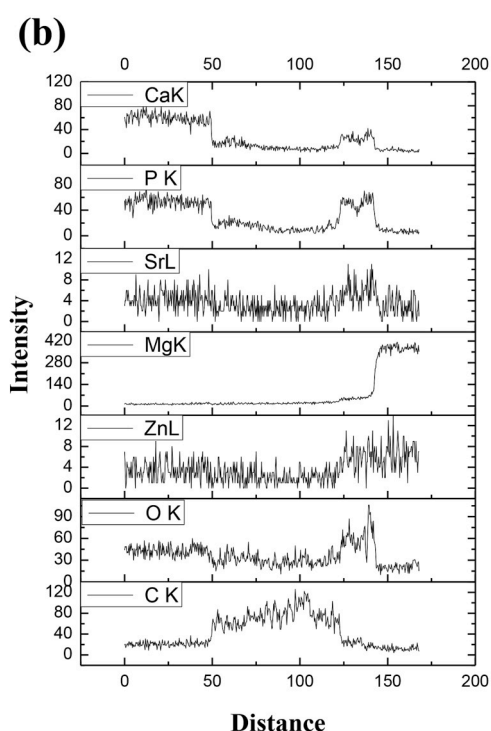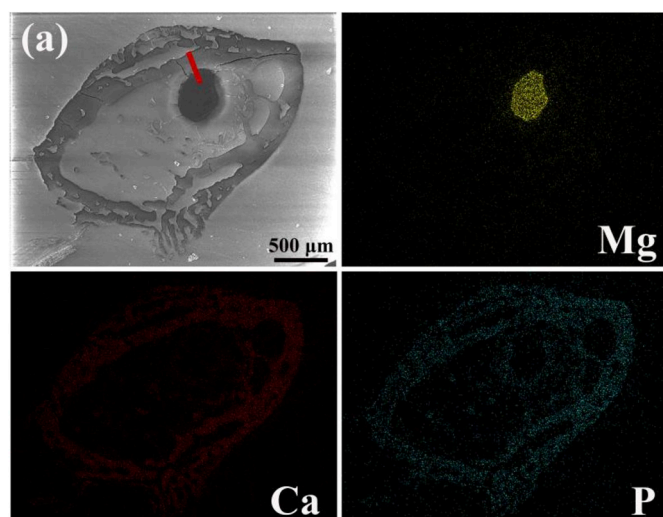
Fig. 10. (a) The element mapping results of cross-section of the mice femoral shaft implanted with Mg–2Sr–Zn rod and (b) the line scan results of marked line in Fig. 10a.

are also better than that of Mg–2Sr alloy. These two alloys can stimulate bone mineralization and promote peri-implant new bone formation without inducing significant adverse effects.

CRediT authorship contribution statement

Kai Chen: Formal analysis, Writing - original draft. **Xinhui Xie:** Formal analysis. **Hongyan Tang:** Formal analysis. **Hui Sun:** Formal analysis. **Ling Qin:** Supervision. **Yufeng Zheng:** Supervision. **Xuenan Gu:** Writing - original draft. **Yubo Fan:** Supervision.

Declaration of competing interest

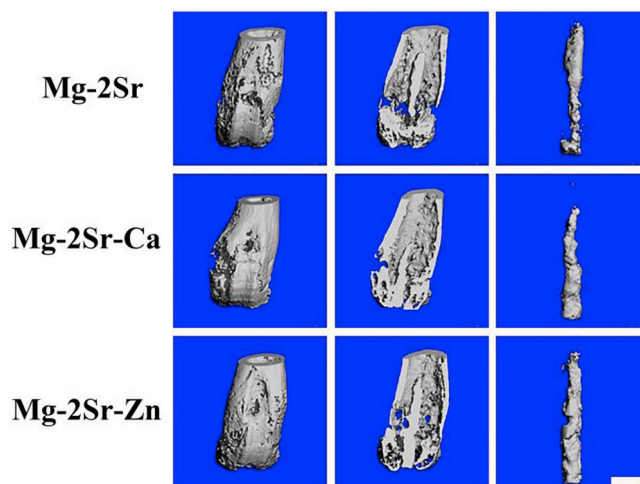The authors declare that they have no conflict of interest.

Fig. 11. The 3-D micro-CT photographs of mice femora and intramedullary Mg–2Sr, Mg–2Sr–Ca and Mg–2Sr–Zn pins 4 weeks post-implantation. The bar length is 1.0 mm.
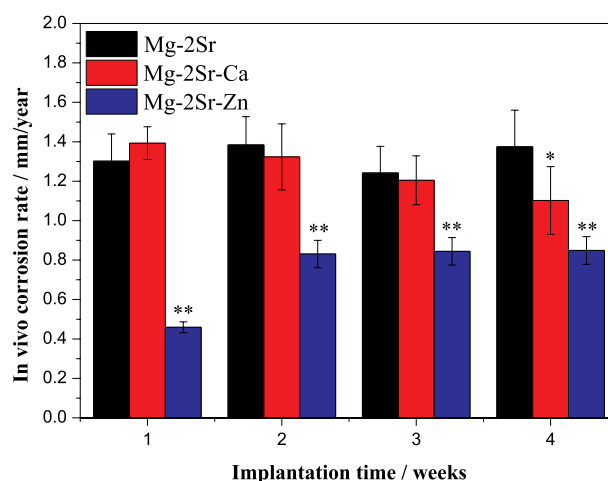

Fig. 12. The *in vivo* degradation rate of Mg–2Sr–Zn and Mg–2Sr–Ca pins during 4 weeks implantation in comparison with Mg–2Sr alloys. $*P < 0.05$ and $**P < 0.01$.

References

[1] Y. Liu, Y. Zheng, X.H. Chen, J.A. Yang, H. Pan, D. Chen, L. Wang, J. Zhang, D. Zhu, S. Wu, K.W.K. Yeung, R.C. Zeng, Y. Han, S. Guan, Fundamental theory of biodegradable metals—definition, criteria, and design, Adv. Funct. Mater. 29 (18) (2019) 1805402.
[2] Y.F. Zheng, X.N. Gu, F. Witte, Biodegradable metals, Mater. Sci. Eng. R Rep. 77 (2014) 1–34.
[3] P. Ding, Y. Liu, X. He, D. Liu, M. Chen, In vitro and in vivo biocompatibility of Mg–Zn–Ca alloy operative clip, Bioactive Materials 4 (2019) 236–244.
[4] S. Wang, X. Zhang, J. Li, C. Liu, S. Guan, Investigation of Mg–Zn–Y–Nd alloy for potential application of biodegradable esophageal stent material, Bioactive Materials 5 (2020) 1–8.
[5] C. Chen, J. Chen, W. Wu, Y. Shi, L. Jin, L. Petrini, L. Shen, G. Yuan, W. Ding, J. Ge, E.R. Edelman, F. Migliavacca, In vivo and in vitro evaluation of a biodegradable magnesium vascular stent designed by shape optimization strategy, Biomaterials

221 (2019) 119414.

[6] R. Hou, J. Victoria-Hernandez, P. Jiang, R. Willumeit-Romer, B. Luthringer-Feyerabend, S. Yi, D. Letzig, F. Feyerabend, In vitro evaluation of the ZX11 magnesium alloy as potential bone plate: degradability and mechanical integrity, Acta Biomater. 97 (2019) 608–622.

[7] A. Krause, N. von der Höh, D. Bormann, C. Krause, F.-W. Bach, H. Windhagen, A. Meyer-Lindenberg, Degradation behaviour and mechanical properties of magnesium implants in rabbit tibiae, J. Mater. Sci. 45 (3) (2010) 624–632.

[8] L. Tan, Q. Wang, X. Lin, P. Wan, G. Zhang, Q. Zhang, K. Yang, Loss of mechanical properties in vivo and bone-implant interface strength of AZ31B magnesium alloy screws with Si-containing coating, Acta Biomater. 10 (5) (2014) 2333–2340.

[9] X.N. Gu, X.H. Xie, N. Li, Y.F. Zheng, L. Qin, In vitro and in vivo studies on a Mg-Sr binary alloy system developed as a new kind of biodegradable metal, Acta Biomater. 8 (6) (2012) 2360–2374.

[10] M. Bornapour, N. Muja, D. Shum-Tim, M. Cerruti, M. Pekguleryuz, Biocompatibility and biodegradability of Mg-Sr alloys: the formation of Sr-substituted hydroxyapatite, Acta Biomater. 9 (2) (2013) 5319–5330.

[11] C. Zhao, F. Pan, L. Zhang, H. Pan, K. Song, A. Tang, Microstructure, mechanical properties, bio-corrosion properties and cytotoxicity of as-extruded Mg-Sr alloys, Mater Sci Eng C Mater Biol Appl 70 (2017) 1081–1088.

[12] Y. Wang, D. Tie, R. Guan, N. Wang, Y. Shang, T. Cui, J. Li, Microstructures, mechanical properties, and degradation behaviors of heat-treated Mg-Sr alloys as potential biodegradable implant materials, J Mech Behav Biomed Mater 77 (2018) 47–57.

[13] I.S. Berglund, H.S. Brar, N. Dolgova, A.P. Acharya, B.G. Keselowsky, M. Sarntinoranont, M.V. Manuel, Synthesis and characterization of Mg-Ca-Sr alloys for biodegradable orthopedic implant applications, J. Biomed. Mater. Res. B Appl. Biomater. 100B (2012) 1524–1534.

[14] M. Li, P. He, Y. Wu, Y. Zhang, H. Xia, Y. Zheng, Y. Han, Stimulatory effects of the degradation products from Mg-Ca-Sr alloy on the osteogenesis through regulating ERK signaling pathway, Sci. Rep. 6 (2016) 32323.

[15] W. Jiang, A.F. Cipriano, Q. Tian, C. Zhang, M. Lopez, A. Sallee, A. Lin, M.C. Cortez Alcaraz, Y. Wu, Y. Zheng, H. Liu, In vitro evaluation of MgSr and MgCaSr alloys via direct culture with bone marrow derived mesenchymal stem cells, Acta Biomater. 72 (2018) 407–423.

[16] P.J. Marie, The calcium-sensing receptor in bone cells: a potential therapeutic target in osteoporosis, Bone 46 (3) (2010) 571–576.

[17] E. Mostaed, M. Sikora-Jasinska, J.W. Drelich, M. Vedani, Zinc-based alloys for degradable vascular stent applications, Acta Biomater. 71 (2018) 1–23.

[18] P.K. Bowen, E.R. Shearier, S. Zhao, R.J. Guillory 2nd, F. Zhao, J. Goldman, J.W. Drelich, Biodegradable metals for cardiovascular stents: from clinical concerns to recent Zn-alloys, Adv Healthc Mater 5 (10) (2016) 1121–1140.

[19] D. Hernández-Escobar, S. Champagne, H. Yilmazer, B. Dikici, C.J. Boehlert, H. Hermawan, Current status and perspectives of zinc-based absorbable alloys for biomedical applications, Acta Biomater. 97 (2019) 1–22.

[20] L.N. Wang, Y. Meng, L.J. Liu, C.F. Dong, Y. Yan, Research progress on biodegradable zinc-based biomaterials, Acta Metall. Sin. 53 (10) (2017) 1317–1322.

[21] L. Wei, J. Li, Y. Zhang, H. Lai, Effects of Zn content on microstructure, mechanical and degradation behaviors of Mg-xZn-0.2Ca-0.1Mn alloys, Mater. Chem. Phys. 241 (2020) 122441.

[22] Z. Li, X. Gu, S. Lou, Y. Zheng, The development of binary Mg-Ca alloys for use as biodegradable materials within bone, Biomaterials 29 (2008) 1329–1344.

[23] M. Bornapour, M. Celikin, M. Cerruti, M. Pekguleryuz, Magnesium implant alloy with low levels of strontium and calcium: the third element effect and phase selection improve bio-corrosion resistance and mechanical performance, Mater. Sci. Eng. C 35 (2014) 267–282.

[24] H.S. Brar, J. Wong, M.V. Manuel, Investigation of the mechanical and degradation properties of Mg-Sr and Mg-Zn-Sr alloys for use as potential biodegradable implant materials, J Mech Behav Biomed Mater 7 (2012) 87–95.

[25] G. He, Y. Wu, Y. Zhang, Y. Zhu, Y. Liu, N. Li, M. Li, G. Zheng, B. He, Q. Yin, Y. Zheng, C. Mao, Addition of Zn to the ternary Mg-Ca-Sr alloys significantly improves their antibacterial property, J. Mater. Chem. B 3 (32) (2015) 6676–6689.

[26] American Society for Testing and Materials, ASTM-G102-89: Standard Practice for Calculation for Corrosion Rates and Related Information from Electrochemical Measurements, Annual Book of ASTM Standards, American Society for Testing and Materials, Philadelphia, PA, USA, 2010.

[27] American Society for Testing and Materials, ASTM-G31-72: Standard Practice for Laboratory Immersion Corrosion Testing of Metals, Annual Book of ASTM Standards, American Society for Testing and Materials, Philadelphia, PA, 2004.

[28] K. Chen, J. Dai, X. Zhang, Improvement of corrosion resistance of magnesium alloys for biomedical applications, Corrosion Rev. 33 (3–4) (2015) 101–117.

[29] X. Zhang, J. Dai, Q. Dong, Z. Ba, Y. Wu, Corrosion behavior and mechanical degradation of as-extruded Mg-Gd-Zn-Zr alloys for orthopedic application, J. Biomed. Mater. Res. B Appl. Biomater. (2019) 1–11.

[30] W.S. Siu, L. Qin, W.H. Cheung, K.S. Leung, A study of trabecular bones in ovariectomized goats with micro-computed tomography and peripheral quantitative computed tomography, Bone 35 (1) (2004) 21–26.

[31] Y. Wu, G. He, Y. Zhang, Y. Liu, M. Li, X. Wang, N. Li, K. Li, G. Zheng, Y. Zheng, Q. Yin, Unique antitumor property of the Mg-Ca-Sr alloys with addition of Zn, Sci. Rep. 6 (2016) 21736.

[32] J. Wang, Y. Wu, H. Li, Y. Liu, X. Bai, W. Chau, Y. Zheng, L. Qin, Magnesium alloy based interference screw developed for ACL reconstruction attenuates peri-tunnel bone loss in rabbits, Biomaterials 157 (2018) 86–97.

[33] H.F. Li, X.H. Xie, Y.B. Wang, Y.F. Zheng, W.H. Wang, L. Qin, In vitro and in vivo studies on biodegradable CaMgZnSrYb high-entropy bulk metallic glass, Acta Biomater. 9 (10) (2013) 8561–8573.

[34] Y. Chen, Z. Xu, C. Smith, J. Sankar, Recent advances on the development of magnesium alloys for biodegradable implants, Acta Biomater. 10 (11) (2014) 4561–4573.

[35] M. Erinc, W.H. Sillekens, R.G.T.M. Mannens, R.J. Werkhoven, Applicability of existing magnesium alloys as biomedical implant materials, Magnesium Technology (2009) 209–214.

[36] E. Zhang, L. Yang, J. Xu, H. Chen, Microstructure, mechanical properties and bio-corrosion properties of Mg–Si(–Ca, Zn) alloy for biomedical application, Acta Biomater. 6 (5) (2010) 1756–1762.

[37] S. Cai, T. Lei, N. Li, F. Feng, Effects of Zn on microstructure, mechanical properties and corrosion behavior of Mg–Zn alloys, Mater. Sci. Eng. C 32 (8) (2012) 2570–2577.

[38] Z. Shi, M. Liu, A. Atrens, Measurement of the corrosion rate of magnesium alloys using Tafel extrapolation, Corrosion Sci. 52 (2010) 579–588.

[39] A.H.M. Sanchez, B.J.C. Luthringer, F. Feyerabend, R. Willumeit, Mg and Mg alloys: how comparable are in vitro and in vivo corrosion rates? A review, Acta Biomater. 13 (2015) 16–31.

[40] E. Willbold, K. Kalla, I. Bartsch, K. Bobe, M. Brauneis, S. Remennik, D. Shechtman, J. Nellesen, W. Tillmann, C. Vogt, F. Witte, Biocompatibility of rapidly solidified magnesium alloy RS66 as a temporary biodegradable metal, Acta Biomater. 9 (10) (2013) 8509–8517.

[41] X. Gu, F. Wang, X. Xie, M. Zheng, P. Li, Y. Zheng, L. Qin, Y. Fan, In vitro and in vivo studies on as-extruded Mg- 5.25wt.%Zn-0.6wt.%Ca alloy as biodegradable metal, Science China Materials 61 (4) (2018) 619–628.

[42] S. Zhang, X. Zhang, C. Zhao, J. Li, Y. Song, C. Xie, H. Tao, Y. Zhang, Y. He, Y. Jiang, Y. Bian, Research on an Mg–Zn alloy as a degradable biomaterial, Acta Biomater. 6 (2) (2010) 626–640.

[43] S.F. Fischerauer, T. Kraus, X. Wu, S. Tangl, E. Sorantin, A.C. Hänzi, J.F. Löffler, P.J. Uggowitzer, A.M. Weinberg, In vivo degradation performance of micro-arc-oxidized magnesium implants: a micro-CT study in rats, Acta Biomater. 9 (2) (2013) 5411–5420.

[44] D. Tie, R. Guan, H. Liu, A. Cipriano, Y. Liu, Q. Wang, Y. Huang, N. Hort, An in vivo study on the metabolism and osteogenic activity of bioabsorbable Mg–1Sr alloy, Acta Biomater. 29 (2016) 455–467.

[45] W. Jiang, A.F. Cipriano, Q. Tian, C. Zhang, M. Lopez, A. Sallee, A. Lin, M.C. Cortez Alcaraz, Y. Wu, Y. Zheng, H. Liu, In vitro evaluation of MgSr and MgCaSr alloys via direct culture with bone marrow derived mesenchymal stem cells, Acta Biomater. 72 (2018) 407–423.

[46] H.F. Li, X.H. Xie, Y.F. Zheng, Y. Cong, F.Y. Zhou, K.J. Qiu, X. Wang, S.H. Chen, L. Huang, L. Tian, L. Qin, Development of biodegradable Zn-1X binary alloys with nutrient alloying elements Mg, Ca and Sr, Sci. Rep. 5 (2015) 10719.

[47] M. Esmaily, J.E. Svensson, S. Fajardo, N. Birbilis, G.S. Frankel, S. Virtanen, R. Arrabal, S. Thomas, L.G. Johansson, Fundamentals and advances in magnesium alloy corrosion, Prog. Mater. Sci. 89 (2017) 92–193.

[48] H. Li, H. Yang, Y. Zheng, F. Zhou, K. Qiu, X. Wang, Design and characterizations of novel biodegradable ternary Zn-based alloys with IIA nutrient alloying elements Mg, Ca and Sr, Mater. Des. 83 (2015) 95–102.